Radiation Physics and Chemistry 159 (2019) 138–146

Contents lists available at ScienceDirect

Radiation Physics and Chemistry

journal homepage: www.elsevier.com/locate/radphyschem

Conversion Coefficients of equivalent and effective doses in terms of air kerma for computational scenarios of Total Body Irradiation in lying-down patients

J.S. Cunha[a,*], W.S. Santos[b,c], A.B. Carvalho Júnior[a]

[a] Universidade Federal de Sergipe, São Cristóvão, SE, Brazil
[b] Instituto de Física, Universidade Federal de Uberlândia, Uberlândia, MG, Brazil
[c] Instituto de Pesquisas Energéticas e Nucleares, Comissão Nacional de Energia Nuclear, São Paulo, SP, Brazil

ARTICLE INFO

Keywords:
Conversion Coefficients
Total Body Irradiation
UF phantom

ABSTRACT

This study aimed to calculate the Conversion Coefficients (CC) of Equivalent and Effective doses by air kerma considering Total Body Irradiation scenarios with Varian linear accelerator with photon beams energy of 4, 6, 10, 15, 18, and 25 MV. The simulations were performed in the MCNPX code and the University of Florida (UF) phantoms were used to represent exposed lying down adult patients in the AP, PA, RLAT, and LLAT irradiation geometries. Lead attenuators were inserted in the scenarios for the preservation of organs of risk and their contribution were analyzed for CC. For most counts, the statistical uncertainty was approximately 5%. For the gonads, CC values for the male phantom decreased with the increase of energy in the AP geometry, which did not occur for the female phantom. As the beam becomes more penetrating, the ovary absorbs more energy because of its internal position. Considering the lung, an organ of risk in TBI, the insertion of the attenuators in the scenarios caused the CC values to reduce by more than 30%. For organs and tissues such as skin and male breasts, the attenuators caused the dose to increase. As for the active bone marrow, which is the TBI target tissue, it was not possible to obtain a good estimate for CC at 15, 18, and 25 MV due to a limitation of the method used to calculate the dose in the bone areas. Nevertheless, for lower energies the CC values for the marrow were valid.

1. Introduction

Due to the biological risks associated with exposures to ionizing radiation, the International Commission on Radiological Protection (ICRP) sets dose limits to prevent these effects from being manifested, such as tissue reactions or stochastic effects (ICRP, 2007). Although dose limits do not apply to medical exposures, the equivalent and effective doses calculation allows the assessment of the probability of deterioration and death. This is relevant for estimating risks in Total Body Irradiation (TBI) treatments. This type of radiation therapy is used for patients diagnosed with leukemia, Hodgkin's lymphoma, and other diseases that require bone marrow transplantation (Van Dyk et al., 1986).

In TBI procedures, the target tissue is the active bone marrow, which is responsible for the production of blood cells. The purpose of the treatment is to destroy the marrow and decrease the immune response of the patient so that rejection is avoided. For this to be achieved, the entire body of the patient is exposed to a beam of photons, usually of high energy, seeking to achieve dose uniformity of approximately 10%, while preserving risky organs, such as the lungs (Van Dyk et al., 1986).

Thomas et al. (2001) analyzed the effects of TBI in adult patients and observed pulmonary complications in 19% of the cases due to patient position and/or beam energy. These effects were more present in patients treated in dorsal and ventral decubitus using a beam of 15 MV compared to patients irradiated laterally with a beam of 9 MV. However, the authors did not study which of these two parameters was the predominant one for the appearance of these complications.

Quast (1987) reported physical and technical aspects of TBI, showing that beam geometry also interferes with dose distribution. It was observed that lateral irradiation does not result in good dose uniformity; therefore, the anteroposterior and posteroanterior irradiation are adopted more frequently.

In this sense, the use of human anatomical models associated with radiation transport codes allows the determination of protection quantities for TBI scenarios (Chakarova et al., 2013; Yao et al., 2012;

* Corresponding author.
E-mail addresses: scjulyanne@gmail.com (J.S. Cunha), william@ufu.br (W.S. Santos), ablohem@gmail.com (A.B. Carvalho Júnior).

https://doi.org/10.1016/j.radphyschem.2019.02.051
Received 26 October 2018; Received in revised form 25 February 2019; Accepted 27 February 2019
Available online 28 February 2019
0969-806X/

Corns et al., 2000). Although the Equivalent and Effective doses are not measurable, it is possible to obtain them using Conversion Coefficients, which are normalized by air kerma, commonly determined by measuring the amount of ionization produced by the photon beam in air (ICRP, 2010).

Thus, this study aimed to calculate Conversion Coefficients of Equivalent and Effective doses using air Kerma for TBI computational scenarios using the MCNPX (version 2.7.0) radiation transport code and the University of Florida (UF) adult male (UFHADM) and female anthropomorphic phantoms (UFHADF) in the vertical position. For these scenarios, our interest was to evaluate the variations in the Conversion Coefficients for Varian linear accelerator spectra (maximum energies of 4, 6, 10, 15, 18, and 25 MV), irradiation geometries, and the influence of the use of irradiation attenuators for the preservation of some regions of the body.

2. Materials and methods

The TBI computational scenarios were simulated in the MCNPX radiation transport code version 2.7.0 (Pelowitz, 2011). We used the University of Florida anthropomorphic computer phantoms for male (UFHADM) and female (UFHADF) adults in vertical position (Lee et al., 2007, 2010). The characteristics of these phantoms are shown in Table 1. They are classified as BREP (boundary representation) because they are created from computed tomography images with image enhancement by the NURBS platform (Xu and Eckerman, 2010). The definition of the internal structures of the phantoms follows the recommendations of the ICRP 89 (ICRP, 2002), which guarantees a good approximation with the reference phantoms (ICRP, 2010).

The estimated energy deposited in the organs was counted from the tally *F8 (MeV/particle) of the code. The energy deposited by photons and electrons was considered, disregarding the kerma approximation. These results were divided by the mass of each organ and multiplied by the factor 1.6×10^{-10}, which converts MeV/g to J/kg, to calculate the average absorbed dose. As in the UF phantom the segmentation of the bone structures is not represented in detail (Lee et al., 2007, 2010), the dose estimation in the Active Bone Marrow and Endosteum in the spongy bone sites and medullary cavities was performed from a conversion method (ICRP, 2010). In these structures, the fluence of photons was calculated using tally F4 (MeV/cm^2/particle) and the card dose-response functions (DE/DF) of the code was used to convert the energy absorbed to dose (ICRP, 2010).

For the simulations, the reliability of the estimates depended on the reliable geometric representation of the computational scenario, the physical model and, in addition to other factors, on the number of "histories" defined in the MCNPX (Pelowitz, 2011). For the relative error to be considerable, a total of 10^8 photons histories were executed.

The following Varian linear accelerator beams were used: 4, 6, 10, 15, 18, and 25 MV (Sheikh-Bagheri and Rogers, 2002). For the scenarios, the source of photons was defined as punctual and emits particles isotropically along the x-axis at a solid angle specified by field size and focal length (Soto-Bernal et al., 2017). The beam was collimated by a lead window (11.3 g/cm^3) as shown in Fig. 1a. The photons and secondary particles that interact with the collimator structure are not followed in the simulation in order to reduce computational time. The linear accelerator structure shown in the figure is only representative.

Table 1
Characteristics of the UF phantom.

	UFHADF	UFHADM
Height	164.7 cm	175.8 cm
Slices	549	586
Lines	166	194
Columns	104	104

In the scenarios, the phantoms were positioned at 400 cm from the source (Lamichhane et al., 2016; Ganapathy et al., 2016), which represents the distance established up to the sagittal plane of the phantom (Chakarova et al., 2013; Bailey et al., 2015). Irradiation was carried out in the anteroposterior (AP), posteroanterior (PA), left lateral (LLAT), and right lateral (RLAT). The area (180×60 cm^2) of the field at this distance was maintained the same for the male and female phantoms.

The height at which the phantoms are positioned on the z-axis is defined so that the source is centered approximately at the navel height, where the dose is prescribed in TBI procedures (Lavallee et al., 2011; Bailey et al., 2015). Following Chakarova et al. (2013) the patient should be kept within 100 cm of the walls to avoid backscatter contributions in this type of procedure.

According to the recommendation 17 of the AAPM, some regions of the body such as head, neck, thorax, legs, and feet need the use of attenuators for radiation shielding (Van Dyk et al., 1986). These objects were modeled as rectangular cells following the thicknesses mentioned in the publication and size according to the organs of the phantoms used in the scenarios, as shown in Fig. 1. According to Narayanasamy et al (2016), the positioning of the attenuators is made in an acrylic holder (1.19 g/cm^3), 1.3 cm thick, placed 16 cm apart from the patient. In order to evaluate the contribution of this to the Conversion Coefficients, all scenarios were modeled with and without these structures.

The results obtained for the average absorbed dose are replaced in Eq. (1) for the calculation of the Equivalent dose. As for photons and electrons, which were the simulated particles, the values of the radiation weighting factors (w_R) are numerically equal to one, the result obtained for the absorbed dose ($D_{T,R}$) has the same value as the equivalent dose (H_T).

$$H_T = \sum_R w_R D_{T,R} \tag{1}$$

These quantities were calculated for both the male H_T^M and the female phantom H_T^F, which allowed the calculation of the effective dose (E), using Eq. (2).

$$E = \sum_T w_T \left[\frac{H_T^M + H_T^F}{2} \right] \tag{2}$$

As recommended by ICRP 116 (ICRP, 2010), the measurable quantity calculated for the normalization of results was the air kerma. This quantity is estimated in the MCNPX in an air cell of 0.6 cm^3, 100 cm from the source by using tally F6 (MeV/g/particle), which considers the kerma approximation.

3. Results and discussion

For most of the results, the statistical uncertainty was approximately 5%. In smaller organs or tissues, counts became more imprecise, less than 10%, which is considered a non-significant error (X-5 Monte Carlo Team, 2003). The source particles interacted less with these structures, thus increasing the relative error in the estimate and consequently the standard deviation (ICRP, 2010). It is important to emphasize that in MCNPX, the standard deviation is given by the product of the mean times the relative error (Pelowitz, 2011).

Fig. 2 shows the results obtained for air kerma per incident particle as a function of the maximum energy of the photon spectra used in the simulations. Air kerma presents a strong dependence on the increase of beam energy, as analyzed by Ounoughi et al. (2015) for X-rays. These values were used to normalize the Equivalent and Effective doses, allowing the results to be presented in the form of Conversion Coefficients (CC), thus eliminating the dependence of the particles from the source for which the quantities in the MCNPX are normalized (X-5 Monte Carlo Team, 2003).

Due to the anatomical distinctions between the UFHADM and UFHADF phantoms, the most discrepant percentage differences

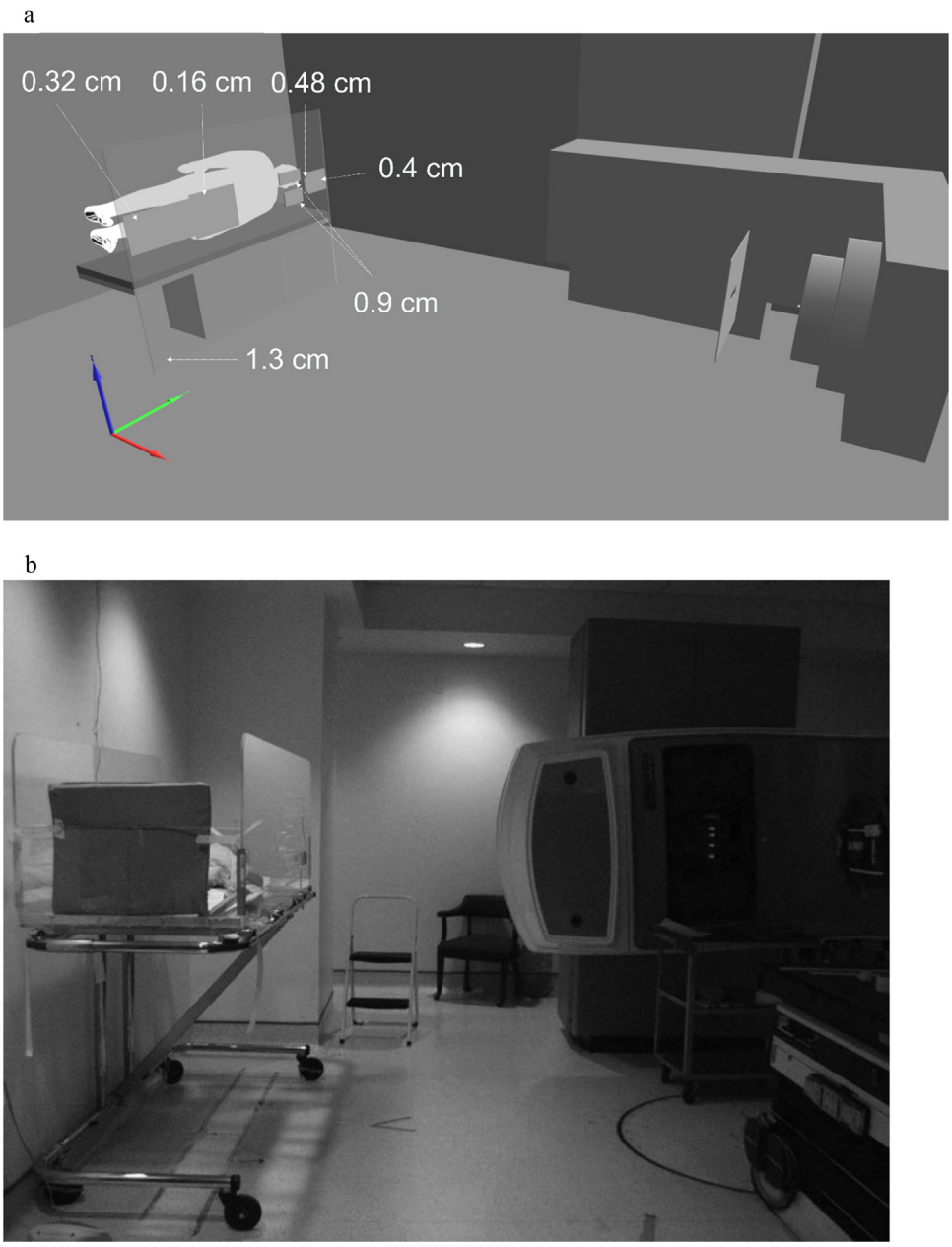

Fig. 1. Comparison between the (a) visualization in Moritz software of the simulated computational scenario and (b) a real TBI scenario (Mesa et al., 2010).

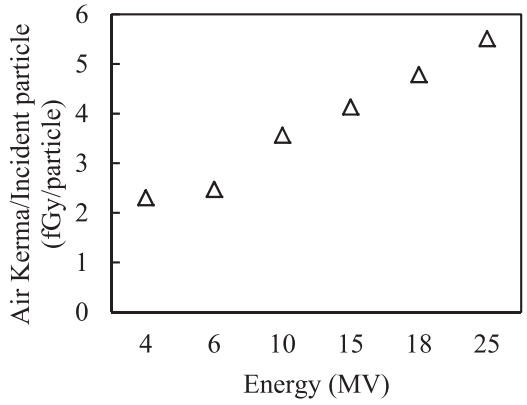

Fig. 2. Air kerma as a function of the maximum energy of the photons spectra of Sheikh-Bagheri and Rogers (2002).

between the CCs of the Equivalent Dose per air kerma H/K_{ar} occurred for the breasts and gonads. In the AP projection, these organs are more exposed, absorbing more energy and causing the CC to be superior to those obtained for the other projections. Fig. 3 shows the CC for the gonads when assuming the AP and PA projections. For the UFHADM phantom, the CC decreased with energy due to the increase of the kerma. However, an opposite behavior was observed for the CC of the UFHADF phantom (Fig. 3a). As the beam becomes more penetrating, the secondary particles will deposit energy at a greater depth. Ovaries absorb a larger dose of energy because they are positioned more internally. When the attenuators were inserted in the scenario, the most significant percentage difference in the CC for the UFHADM phantom was 18.4% for the 25 MV beam. This shielding is performed by the influence of the attenuator that was positioned over the region of the legs.

For the PA geometry, all CCs for both phantoms showed increasing behavior (Fig. 3b). The insertion of attenuators caused a reduction of the coefficients of less than 5% for the UFHADM phantom and the

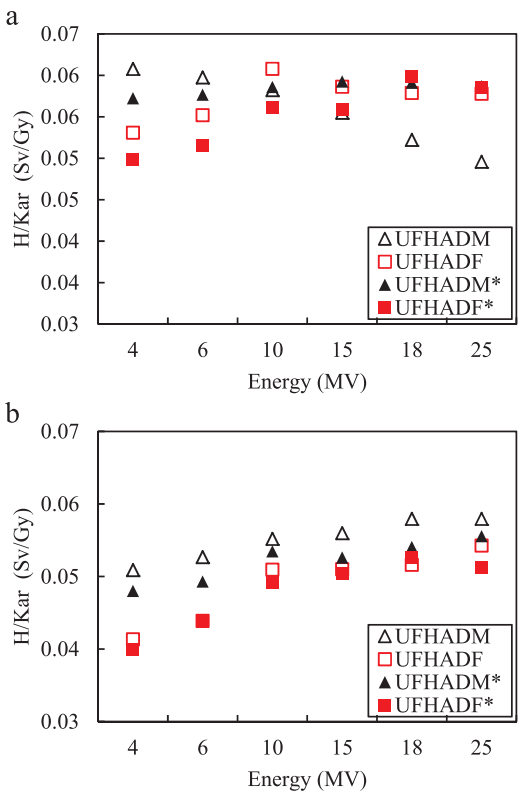

Fig. 3. H/K_{ar} Conversion Coefficients for the gonads in the irradiation geometries (a) AP and (b) PA. Curves named as UFHADM* and UFHADF* refer to scenarios using attenuators.

differences are irrelevant for UFHADF. The phantom body plays the role of the shielding for the gonads in this irradiation geometry.

As expected, female breasts have higher CC values than male breasts because of the larger volume. Only for the 4 MV beam, the percentage difference between the CC for UFHADF and UFHADM assumed a minimum value of 2%. For higher energies, the coefficients decreased due to the increased kerma. This is more expressive for the UFHADM phantom because the more energetic the beam becomes, the less energy is deposited in superficial organs such as the breasts, reaching a difference of 34.2% in relation to the female for the 25 MV beam. ICRP (2010) points out that the energy of the photons and the depth of the organs of the body are important parameters that influence the values of the Conversion Coefficients.

There was a change in the behavior of the CC values in the AP geometry when the attenuators were inserted in the scenario (Fig. 4). The maximum percentage differences occurred for the 4 MV beam,

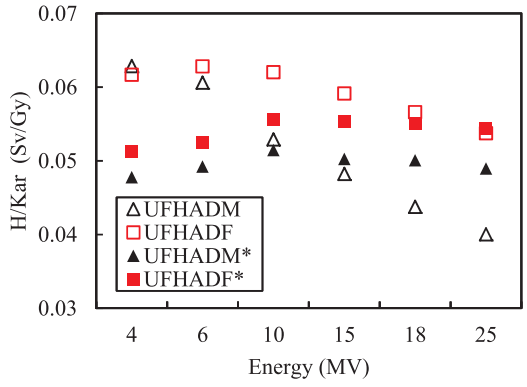

Fig. 4. H/K_{ar} Conversion Coefficients for the breasts in the AP irradiation geometry.

which was 24% for the male phantom and 17% for the female one. The decrease in CC was more significant for the male phantom because attenuators of the same thickness (0.9 cm) were used in both cases. The attenuators caused the lower energy radiation to be filtered, leading to the hardening of the beam and causing more external organs to absorb a lower dose. Thus, shielding affects more the male breasts because they have a smaller volume. The percentage difference between the CCs for the UFHADF phantom became smaller with energy increase, reaching a minimum difference of 1% for the 25 MV beam. The influence of shielding became even less significant for the UFHADF phantom in the lateral geometries. Although Lee et al. (2010) evidenced that female breasts in the UF phantoms were remodeled to have a more asymmetrical shape, and the CC for RLAT and LLAT remained constant.

For the lungs, CC values increased for all irradiation geometries with increasing photon beam energy. The internal region of the lungs of the UF phantoms, where the photons interact, is filled with a material with a density of 0.33 g/cm^3, according to the recommendations of ICRP 89 (2002). The shielding causes the CC to reduce by approximately 30%, reaching greater percentage differences for lateral projections (up to 36% for RLAT). The phantom arms lead to a partial attenuation of the radiation in this organ because they are positioned adjacent to the body (Mesa et al., 2010).

Attenuators were positioned in front of the head (0.4 cm thick) and neck (0.48 cm thick) regions, which leads to the reduction of CC to the thyroid and salivary glands. For the thyroid, CC values decreased by more than 30% for the lateral irradiation geometries. Since the organ is more exposed in the AP projection, the CC values are higher. Under these exposure conditions, the CC for the male phantom showed a minimum percentage difference of 2% for the 10 MV beam, which was not the case for the female phantom. This is because in the UFHADM phantom the thyroid, in addition to having a larger volume of 19.1 cm^3, which increases the area of interaction, it is positioned closer to the anterior end of the body, as shown in Fig. 5a (Lee et al., 2010). In the UFHADF phantom, there was a thicker layer of adipose tissue, as shown in Fig. 5b, which causes the thyroid to absorb less energy because it is positioned at a greater depth in the body and suffers more influence

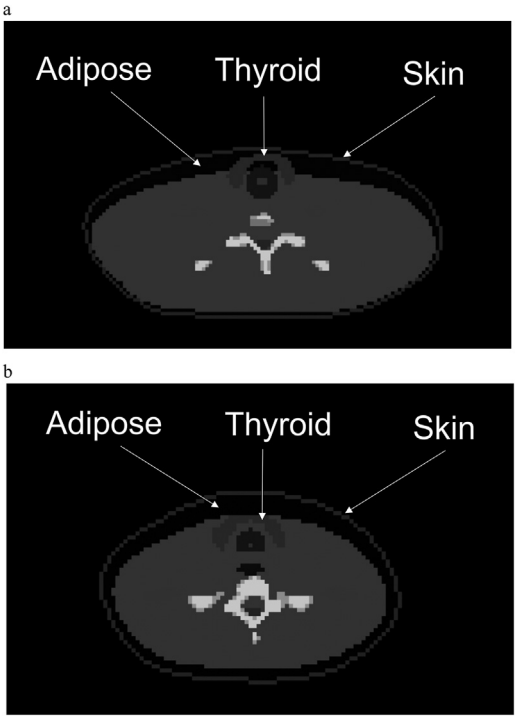

Fig. 5. Image J visualization of a cut in the axial plane of the phantoms (a) UFHADM and (b) UFHADF.

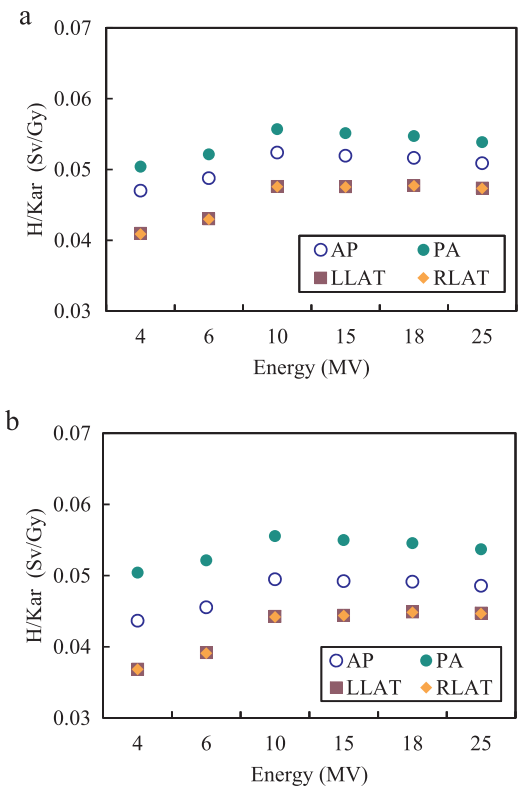

Fig. 6. H/K_{ar} Conversion Coefficients of the UFHADM phantom for (a) Endosteum and (b) Active Bone Marrow.

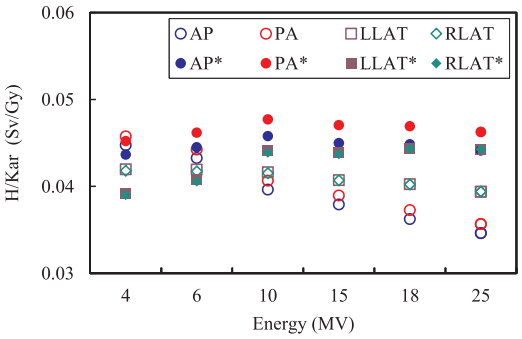

Fig. 7. H/K_{ar} Conversion Coefficients of the UFHADM phantom for skin. The curves named AP*, PA*, LLAT* and RLAT* refer to scenarios using attenuators.

from the attenuators.

For the salivary glands, the presence of the attenuators in the scenario leaded to larger percentage differences for the lateral irradiation geometries. The calculated dose for this tissue includes the sum of the results obtained for the sublingual, submandibular and parotid glands; the parotid glands have a larger volume and are positioned laterally

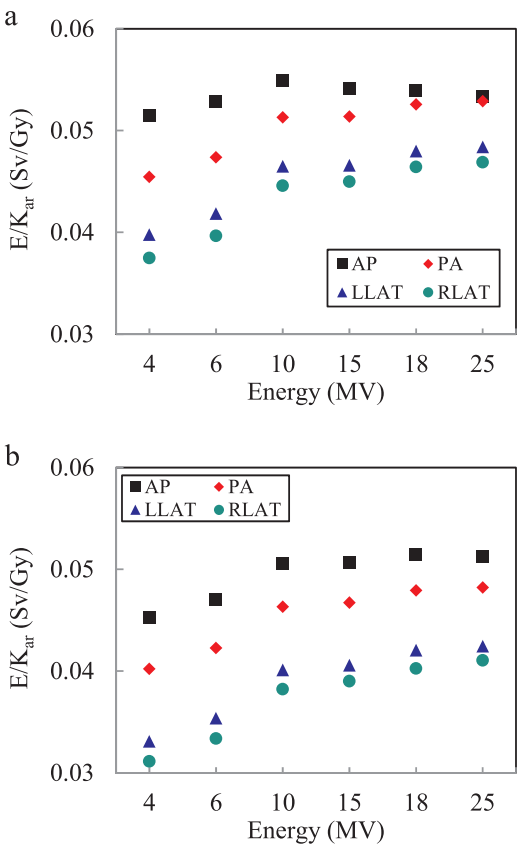

Fig. 9. Comparison between the E/K_{ar} (Sv/Gy) Conversion Coefficients in the computational scenarios (a) without the attenuators and (b) with the attenuators.

(Lee et al., 2010). For the AP projection, a condition in which the sublingual glands are most affected by the shielding, the differences in the CCs showed maximum values of 14% for UFHADM and 19.3% for UFHADF when considering the 4 MV beam. Jones et al. (1992) points out that the reduction of salivary flow and loss of salivary protection, which leads the patient to have pre-disposition to dental caries, are tissue reactions manifested in patients treated by TBI.

For endosteum and active bone marrow, the Conversion Coefficients presented similar behaviors, with maximum values for the 10 MV beam decreased with increasing kerma for both female and male in all geometries of irradiation (Fig. 6). As mentioned by El-Khatib et al. (1992), bone dose reduction is an undesirable effect in TBI since target tissues are located within it, concluding that 18 MV beams would be more suitable for treatment. However, the CC for the scenarios with the 15, 18 and 25 MV showed few variations compared to those obtained for the 10 MV beam due to the response functions used for dose estimation in these structures. The coefficients provided by the ICRP provided dose-flow conversion factors with maximum energy of up to 10 MV

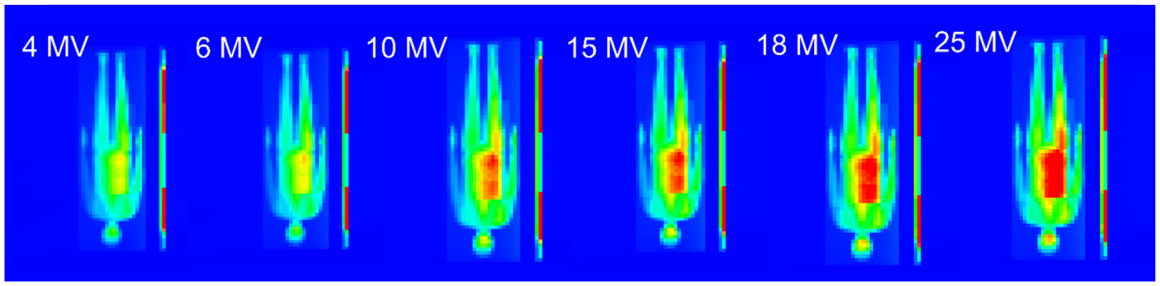

Fig. 8. Visualization in the Moritz software of Mesh tally for the phantom UFHADM in the RLAT projection.

Table 2
H/K_{ar} Conversion Coefficients (Sv/Gy) for the UFHADM phantom.

	4 MV				6 MV				10 MV			
Organ/tissue	**AP**	**PA**	**LLAT**	**RLAT**	**AP**	**PA**	**LLAT**	**RLAT**	**AP**	**PA**	**LLAT**	**RLAT**
Brain	0.043 ± 0.001	0.047 ± 0.001	0.048 ± 0.001	0.048 ± 0.001	0.044 ± 0.001	0.049 ± 0.001	0.050 ± 0.001	0.050 ± 0.001	0.049 ± 0.001	0.053 ± 0.001	0.053 ± 0.001	0.053 ± 0.001
Breasts	0.063 ± 0.002	0.039 ± 0.001	0.046 ± 0.001	0.046 ± 0.002	0.061 ± 0.002	0.041 ± 0.001	0.048 ± 0.002	0.045 ± 0.002	0.053 ± 0.002	0.045 ± 0.001	0.050 ± 0.002	0.050 ± 0.002
Colon	0.055 ± 0.001	0.042 ± 0.001	0.038 ± 0.001	0.039 ± 0.001	0.056 ± 0.001	0.044 ± 0.001	0.040 ± 0.001	0.041 ± 0.001	0.059 ± 0.001	0.048 ± 0.001	0.046 ± 0.001	0.046 ± 0.001
Endosteum	0.047 ± 0.001	0.050 ± 0.001	0.041 ± 0.001	0.041 ± 0.001	0.049 ± 0.001	0.052 ± 0.001	0.043 ± 0.001	0.043 ± 0.001	0.052 ± 0.001	0.056 ± 0.001	0.048 ± 0.001	0.048 ± 0.001
Esophagus	0.045 ± 0.001	0.046 ± 0.001	0.030 ± 0.001	0.030 ± 0.001	0.047 ± 0.001	0.048 ± 0.001	0.032 ± 0.001	0.033 ± 0.001	0.052 ± 0.001	0.051 ± 0.001	0.038 ± 0.001	0.038 ± 0.001
Gonads	0.061 ± 0.002	0.051 ± 0.002	0.032 ± 0.001	0.032 ± 0.001	0.060 ± 0.002	0.053 ± 0.002	0.034 ± 0.001	0.034 ± 0.001	0.058 ± 0.002	0.055 ± 0.002	0.039 ± 0.001	0.039 ± 0.001
Liver	0.049 ± 0.001	0.045 ± 0.001	0.027 ± 0.001	0.042 ± 0.001	0.051 ± 0.001	0.047 ± 0.001	0.029 ± 0.001	0.044 ± 0.001	0.054 ± 0.001	0.051 ± 0.001	0.035 ± 0.001	0.049 ± 0.001
Lungs	0.051 ± 0.001	0.053 ± 0.001	0.035 ± 0.001	0.037 ± 0.001	0.052 ± 0.001	0.054 ± 0.001	0.037 ± 0.001	0.039 ± 0.001	0.056 ± 0.001	0.058 ± 0.001	0.043 ± 0.001	0.045 ± 0.001
Active bone marrow	0.043 ± 0.001	0.047 ± 0.001	0.048 ± 0.001	0.048 ± 0.001	0.044 ± 0.001	0.049 ± 0.001	0.050 ± 0.001	0.050 ± 0.001	0.049 ± 0.001	0.053 ± 0.001	0.053 ± 0.001	0.053 ± 0.001
Remaining tissues	0.049 ± 0.001	0.048 ± 0.001	0.038 ± 0.001	0.036 ± 0.001	0.051 ± 0.001	0.050 ± 0.001	0.040 ± 0.001	0.039 ± 0.001	0.054 ± 0.001	0.054 ± 0.001	0.045 ± 0.001	0.043 ± 0.001
Salivary glands	0.053 ± 0.001	0.052 ± 0.001	0.052 ± 0.001	0.054 ± 0.001	0.055 ± 0.001	0.054 ± 0.001	0.053 ± 0.001	0.055 ± 0.001	0.056 ± 0.001	0.055 ± 0.001	0.054 ± 0.001	0.055 ± 0.001
Skin	0.045 ± 0.001	0.046 ± 0.001	0.042 ± 0.001	0.042 ± 0.001	0.043 ± 0.001	0.044 ± 0.001	0.042 ± 0.001	0.042 ± 0.001	0.040 ± 0.001	0.041 ± 0.001	0.042 ± 0.001	0.042 ± 0.001
Stomach	0.051 ± 0.001	0.044 ± 0.001	0.046 ± 0.001	0.026 ± 0.001	0.053 ± 0.001	0.046 ± 0.001	0.048 ± 0.001	0.028 ± 0.001	0.056 ± 0.001	0.049 ± 0.001	0.052 ± 0.001	0.035 ± 0.001
Thyroid	0.061 ± 0.002	0.036 ± 0.001	0.038 ± 0.001	0.034 ± 0.001	0.061 ± 0.002	0.039 ± 0.001	0.040 ± 0.002	0.037 ± 0.001	0.057 ± 0.002	0.043 ± 0.002	0.047 ± 0.002	0.042 ± 0.001
Urinary bladder	0.050 ± 0.001	0.044 ± 0.001	0.032 ± 0.001	0.031 ± 0.001	0.052 ± 0.001	0.046 ± 0.001	0.034 ± 0.001	0.034 ± 0.001	0.054 ± 0.001	0.050 ± 0.001	0.040 ± 0.001	0.040 ± 0.001

	15 MV				18 MV				25 MV			
Organ/tissue	**AP**	**PA**	**LLAT**	**RLAT**	**AP**	**PA**	**LLAT**	**RLAT**	**AP**	**PA**	**LLAT**	**RLAT**
Brain	0.049 ± 0.001	0.053 ± 0.001	0.053 ± 0.001	0.053 ± 0.001	0.050 ± 0.001	0.054 ± 0.001	0.054 ± 0.001	0.054 ± 0.001	0.051 ± 0.001	0.054 ± 0.001	0.054 ± 0.001	0.054 ± 0.001
Breasts	0.048 ± 0.001	0.045 ± 0.001	0.049 ± 0.002	0.048 ± 0.001	0.044 ± 0.001	0.046 ± 0.001	0.048 ± 0.001	0.049 ± 0.001	0.040 ± 0.001	0.048 ± 0.001	0.046 ± 0.001	0.047 ± 0.001
Colon	0.058 ± 0.001	0.049 ± 0.001	0.047 ± 0.001	0.047 ± 0.001	0.058 ± 0.001	0.050 ± 0.001	0.048 ± 0.001	0.048 ± 0.001	0.057 ± 0.001	0.051 ± 0.001	0.049 ± 0.001	0.049 ± 0.001
Endosteum	0.052 ± 0.001	0.055 ± 0.001	0.048 ± 0.001	0.048 ± 0.001	0.052 ± 0.000	0.055 ± 0.001	0.048 ± 0.000	0.048 ± 0.000	0.051 ± 0.001	0.054 ± 0.001	0.047 ± 0.000	0.047 ± 0.000
Esophagus	0.050 ± 0.001	0.053 ± 0.001	0.039 ± 0.001	0.039 ± 0.001	0.051 ± 0.001	0.055 ± 0.001	0.040 ± 0.001	0.041 ± 0.001	0.052 ± 0.001	0.055 ± 0.001	0.042 ± 0.001	0.042 ± 0.001
Gonads	0.055 ± 0.002	0.056 ± 0.002	0.039 ± 0.001	0.041 ± 0.001	0.052 ± 0.001	0.058 ± 0.001	0.042 ± 0.001	0.042 ± 0.001	0.050 ± 0.001	0.058 ± 0.001	0.044 ± 0.001	0.043 ± 0.001
Liver	0.054 ± 0.001	0.051 ± 0.001	0.036 ± 0.001	0.049 ± 0.001	0.055 ± 0.001	0.052 ± 0.001	0.038 ± 0.000	0.051 ± 0.001	0.055 ± 0.001	0.053 ± 0.001	0.039 ± 0.000	0.052 ± 0.001
Lungs	0.056 ± 0.001	0.058 ± 0.001	0.044 ± 0.001	0.046 ± 0.001	0.057 ± 0.001	0.060 ± 0.001	0.047 ± 0.000	0.049 ± 0.001	0.058 ± 0.001	0.060 ± 0.001	0.048 ± 0.001	0.049 ± 0.001
Active bone marrow	0.049 ± 0.001	0.053 ± 0.001	0.053 ± 0.001	0.053 ± 0.001	0.050 ± 0.001	0.054 ± 0.001	0.054 ± 0.001	0.054 ± 0.001	0.051 ± 0.001	0.054 ± 0.001	0.054 ± 0.001	0.054 ± 0.001
Remaining tissues	0.054 ± 0.001	0.054 ± 0.001	0.046 ± 0.001	0.044 ± 0.001	0.054 ± 0.001	0.055 ± 0.001	0.047 ± 0.001	0.046 ± 0.001	0.055 ± 0.001	0.055 ± 0.001	0.048 ± 0.001	0.046 ± 0.001
Salivary glands	0.056 ± 0.001	0.055 ± 0.001	0.052 ± 0.001	0.053 ± 0.001	0.055 ± 0.001	0.055 ± 0.001	0.051 ± 0.001	0.052 ± 0.001	0.054 ± 0.001	0.055 ± 0.001	0.051 ± 0.001	0.051 ± 0.001
Skin	0.038 ± 0.001	0.039 ± 0.001	0.041 ± 0.001	0.041 ± 0.001	0.036 ± 0.000	0.037 ± 0.000	0.040 ± 0.000	0.040 ± 0.000	0.035 ± 0.000	0.036 ± 0.000	0.039 ± 0.000	0.039 ± 0.000
Stomach	0.056 ± 0.001	0.049 ± 0.001	0.053 ± 0.001	0.035 ± 0.001	0.057 ± 0.001	0.051 ± 0.001	0.054 ± 0.001	0.038 ± 0.001	0.057 ± 0.001	0.052 ± 0.001	0.054 ± 0.001	0.039 ± 0.001
Thyroid	0.054 ± 0.002	0.044 ± 0.001	0.046 ± 0.002	0.044 ± 0.002	0.051 ± 0.001	0.046 ± 0.001	0.047 ± 0.001	0.047 ± 0.001	0.049 ± 0.001	0.046 ± 0.001	0.049 ± 0.001	0.045 ± 0.001
Urinary bladder	0.056 ± 0.001	0.050 ± 0.001	0.041 ± 0.001	0.041 ± 0.001	0.057 ± 0.001	0.052 ± 0.001	0.043 ± 0.001	0.043 ± 0.001	0.057 ± 0.001	0.053 ± 0.001	0.044 ± 0.001	0.044 ± 0.001

Table 3
H/K_{ar} Conversion Coefficients (Sv/Gy) for the UFHADF phantom.

	4 MV				6 MV				10 MV			
Organ/tissue	**AP**	**PA**	**LLAT**	**RLAT**	**AP**	**PA**	**LLAT**	**RLAT**	**AP**	**PA**	**LLAT**	**RLAT**
Brain	0.043 ± 0.001	0.047 ± 0.001	0.049 ± 0.001	0.049 ± 0.001	0.045 ± 0.001	0.049 ± 0.001	0.051 ± 0.001	0.051 ± 0.001	0.050 ± 0.001	0.053 ± 0.001	0.054 ± 0.001	0.054 ± 0.001
Breasts	0.062 ± 0.001	0.035 ± 0.001	0.046 ± 0.001	0.046 ± 0.001	0.063 ± 0.001	0.037 ± 0.001	0.048 ± 0.001	0.048 ± 0.001	0.062 ± 0.001	0.043 ± 0.001	0.051 ± 0.001	0.051 ± 0.001
Colon	0.052 ± 0.001	0.043 ± 0.001	0.040 ± 0.001	0.040 ± 0.001	0.054 ± 0.001	0.045 ± 0.001	0.042 ± 0.001	0.043 ± 0.001	0.057 ± 0.001	0.050 ± 0.001	0.047 ± 0.001	0.047 ± 0.001
Endosteum	0.037 ± 0.001	0.039 ± 0.001	0.033 ± 0.001	0.033 ± 0.001	0.038 ± 0.001	0.041 ± 0.001	0.035 ± 0.001	0.034 ± 0.001	0.041 ± 0.001	0.044 ± 0.001	0.038 ± 0.001	0.038 ± 0.001
Esophagus	0.044 ± 0.001	0.050 ± 0.001	0.037 ± 0.001	0.034 ± 0.001	0.046 ± 0.001	0.051 ± 0.001	0.039 ± 0.001	0.036 ± 0.001	0.050 ± 0.001	0.055 ± 0.001	0.045 ± 0.001	0.041 ± 0.001
Gonads	0.053 ± 0.002	0.041 ± 0.002	0.033 ± 0.002	0.029 ± 0.001	0.055 ± 0.002	0.044 ± 0.002	0.035 ± 0.002	0.032 ± 0.002	0.061 ± 0.002	0.051 ± 0.002	0.041 ± 0.002	0.039 ± 0.002
Liver	0.048 ± 0.001	0.046 ± 0.001	0.032 ± 0.001	0.046 ± 0.001	0.050 ± 0.001	0.047 ± 0.001	0.034 ± 0.001	0.048 ± 0.001	0.054 ± 0.001	0.051 ± 0.001	0.040 ± 0.001	0.052 ± 0.001
Lungs	0.049 ± 0.001	0.052 ± 0.001	0.038 ± 0.001	0.039 ± 0.001	0.051 ± 0.001	0.054 ± 0.001	0.041 ± 0.001	0.042 ± 0.001	0.054 ± 0.001	0.057 ± 0.001	0.046 ± 0.001	0.047 ± 0.001
Active bone marrow	0.043 ± 0.001	0.047 ± 0.001	0.049 ± 0.001	0.049 ± 0.001	0.045 ± 0.001	0.049 ± 0.001	0.051 ± 0.001	0.051 ± 0.001	0.050 ± 0.001	0.053 ± 0.001	0.054 ± 0.001	0.054 ± 0.001
Remaining tissues	0.046 ± 0.001	0.049 ± 0.001	0.042 ± 0.001	0.041 ± 0.001	0.048 ± 0.001	0.051 ± 0.001	0.044 ± 0.001	0.043 ± 0.001	0.052 ± 0.001	0.054 ± 0.001	0.049 ± 0.001	0.047 ± 0.001
Salivary glands	0.049 ± 0.001	0.052 ± 0.001	0.054 ± 0.001	0.054 ± 0.001	0.051 ± 0.001	0.053 ± 0.001	0.056 ± 0.001	0.055 ± 0.001	0.055 ± 0.001	0.057 ± 0.001	0.056 ± 0.001	0.056 ± 0.001
Skin	0.046 ± 0.001	0.047 ± 0.001	0.043 ± 0.001	0.043 ± 0.001	0.045 ± 0.001	0.045 ± 0.001	0.043 ± 0.001	0.043 ± 0.001	0.041 ± 0.001	0.042 ± 0.001	0.043 ± 0.001	0.043 ± 0.001
Stomach	0.051 ± 0.001	0.043 ± 0.001	0.053 ± 0.001	0.030 ± 0.001	0.053 ± 0.001	0.045 ± 0.001	0.054 ± 0.001	0.033 ± 0.001	0.056 ± 0.001	0.049 ± 0.001	0.057 ± 0.001	0.039 ± 0.001
Thyroid	0.059 ± 0.002	0.041 ± 0.002	0.042 ± 0.002	0.042 ± 0.002	0.059 ± 0.002	0.042 ± 0.002	0.043 ± 0.002	0.044 ± 0.002	0.060 ± 0.002	0.047 ± 0.002	0.048 ± 0.002	0.050 ± 0.002
Urinary bladder	0.054 ± 0.001	0.041 ± 0.001	0.035 ± 0.001	0.035 ± 0.001	0.056 ± 0.001	0.043 ± 0.001	0.037 ± 0.001	0.036 ± 0.001	0.058 ± 0.001	0.048 ± 0.001	0.042 ± 0.001	0.042 ± 0.001
	15 MV				**18 MV**				**25 MV**			
Organ/tissue	**AP**	**PA**	**LLAT**	**RLAT**	**AP**	**PA**	**LLAT**	**RLAT**	**AP**	**PA**	**LLAT**	**RLAT**
Brain	0.050 ± 0.001	0.053 ± 0.001	0.054 ± 0.001	0.054 ± 0.001	0.051 ± 0.001	0.054 ± 0.001	0.055 ± 0.001	0.055 ± 0.001	0.052 ± 0.001	0.054 ± 0.001	0.055 ± 0.001	0.055 ± 0.001
Breasts	0.059 ± 0.001	0.043 ± 0.001	0.051 ± 0.001	0.050 ± 0.001	0.057 ± 0.001	0.045 ± 0.001	0.051 ± 0.001	0.051 ± 0.001	0.054 ± 0.001	0.046 ± 0.001	0.050 ± 0.001	0.050 ± 0.001
Colon	0.057 ± 0.001	0.050 ± 0.001	0.047 ± 0.001	0.048 ± 0.001	0.057 ± 0.001	0.051 ± 0.001	0.049 ± 0.001	0.050 ± 0.001	0.057 ± 0.001	0.051 ± 0.001	0.050 ± 0.001	0.050 ± 0.001
Endosteum	0.041 ± 0.001	0.043 ± 0.001	0.038 ± 0.001	0.038 ± 0.001	0.040 ± 0.000	0.043 ± 0.000	0.038 ± 0.000	0.038 ± 0.000	0.040 ± 0.000	0.042 ± 0.000	0.038 ± 0.000	0.038 ± 0.000
Esophagus	0.051 ± 0.001	0.054 ± 0.001	0.046 ± 0.001	0.043 ± 0.001	0.050 ± 0.001	0.055 ± 0.001	0.048 ± 0.001	0.043 ± 0.001	0.053 ± 0.001	0.056 ± 0.001	0.050 ± 0.001	0.045 ± 0.001
Gonads	0.059 ± 0.002	0.051 ± 0.002	0.039 ± 0.002	0.041 ± 0.002	0.058 ± 0.002	0.052 ± 0.002	0.042 ± 0.002	0.044 ± 0.002	0.058 ± 0.002	0.054 ± 0.002	0.043 ± 0.002	0.046 ± 0.002
Liver	0.054 ± 0.001	0.051 ± 0.001	0.041 ± 0.001	0.052 ± 0.001	0.055 ± 0.001	0.053 ± 0.001	0.043 ± 0.000	0.053 ± 0.001	0.055 ± 0.001	0.053 ± 0.001	0.043 ± 0.000	0.054 ± 0.001
Lungs	0.055 ± 0.001	0.058 ± 0.001	0.047 ± 0.001	0.048 ± 0.001	0.056 ± 0.001	0.059 ± 0.001	0.049 ± 0.001	0.050 ± 0.001	0.056 ± 0.001	0.059 ± 0.001	0.050 ± 0.001	0.051 ± 0.001
Active bone marrow	0.050 ± 0.001	0.053 ± 0.001	0.054 ± 0.001	0.054 ± 0.001	0.051 ± 0.001	0.054 ± 0.001	0.055 ± 0.001	0.055 ± 0.001	0.052 ± 0.001	0.054 ± 0.001	0.055 ± 0.001	0.055 ± 0.001
Remaining tissues	0.052 ± 0.001	0.054 ± 0.001	0.049 ± 0.001	0.047 ± 0.001	0.053 ± 0.001	0.055 ± 0.001	0.051 ± 0.001	0.048 ± 0.001	0.053 ± 0.001	0.055 ± 0.001	0.051 ± 0.001	0.049 ± 0.001
Salivary glands	0.054 ± 0.001	0.057 ± 0.001	0.054 ± 0.001	0.054 ± 0.001	0.054 ± 0.001	0.057 ± 0.001	0.053 ± 0.001	0.053 ± 0.001	0.054 ± 0.001	0.057 ± 0.001	0.052 ± 0.001	0.052 ± 0.001
Skin	0.039 ± 0.001	0.040 ± 0.001	0.042 ± 0.001	0.042 ± 0.001	0.037 ± 0.000	0.038 ± 0.000	0.041 ± 0.000	0.041 ± 0.000	0.036 ± 0.000	0.036 ± 0.000	0.040 ± 0.000	0.040 ± 0.000
Stomach	0.056 ± 0.001	0.049 ± 0.001	0.057 ± 0.001	0.039 ± 0.001	0.057 ± 0.001	0.050 ± 0.001	0.059 ± 0.001	0.041 ± 0.001	0.057 ± 0.001	0.051 ± 0.001	0.059 ± 0.001	0.043 ± 0.001
Thyroid	0.060 ± 0.002	0.048 ± 0.002	0.048 ± 0.002	0.050 ± 0.002	0.058 ± 0.002	0.050 ± 0.002	0.052 ± 0.002	0.050 ± 0.002	0.056 ± 0.002	0.050 ± 0.001	0.051 ± 0.002	0.052 ± 0.002
Urinary bladder	0.059 ± 0.001	0.048 ± 0.001	0.043 ± 0.001	0.043 ± 0.001	0.059 ± 0.001	0.049 ± 0.001	0.047 ± 0.001	0.045 ± 0.001	0.058 ± 0.001	0.050 ± 0.001	0.047 ± 0.001	0.045 ± 0.001

(ICRP, 2010).

For skin, CC valued showed decreasing behavior (Fig. 7). The presence of the attenuators and the acrylic carrier increases the probability of interaction of the photons by the photoelectric effect, leading to the increase of the dose in the skin due to released secondary particles (Narayanasamy et al., 2016; Linares et al., 2017). The CCs assumed similar values of approximately 0.04 Sv/Gy, even with the change in irradiation geometry and source.

As the lead attenuators were positioned near the head, neck, thorax, feet and legs regions, the CC of some organs were practically not influenced by their presence in the computational scenario, such as: Bladder, Colon, Stomach, Liver and gonads (except in the AP projection, as already discussed). Fig. 8 shows an image of the exposure scenario obtained with the MCNPX mesh tally. The function was associated with the PEDEP command to estimate the energy deposited for any type of particle considering the kerma approximation in the region of interest (Pelowitz, 2011).

The Conversion Coefficients of the effective dose per air kerma E/K_{ar} are shown in Fig. 8. For scenarios with a beam of up to 10 MV, the CCs showed increasing behavior, where they reached their maximum value for all geometries of irradiation, as shown in Fig. 8a. For higher energies, the effective dose growth is compensated by the growth of the kerma, with values close to 0.06 Sv/Gy for the AP and PA geometries and 0.05 Sv/Gy for the lateral ones. In general, CCs were higher for AP/PA, as already observed in CCs of equivalent dose per air kerma. In addition, the organs that contribute the most to the effective dose, because of their radiosensitivity, absorb more doses in the AP/PA projections, as compared to the active marrow, colon, lung, breasts, and remaining tissues (ICRP, 2007). In this study, the weight factors of the organs/tissues classified as remnants were reweighted since the dose was not calculated in the lymph nodes.

When the attenuators are inserted in the scenario, as shown in Fig. 9b, the percentage differences between the CCs decrease with increasing energy. For the 25 MV beam, the CC became only 4% lower for the AP geometry. The major influences of the attenuators were reflected in the CC for the lateral geometries, for the 4 and 6 MV beams, where they became approximately 16% lower than those shown in Fig. 9a.

As one of our objectives was to provide the equivalent and effective dose CCs per air kerma for TBI scenarios, in Tables 2 and 3 all CCs are presented, in addition to those not explicitly discussed for scenarios without attenuators.

4. Conclusions

For the exposure conditions adopted in this study, the Conversion Coefficients of equivalent dose per kerma suffered a strong dependence of the source energy, beam projection and distribution of the organs in the body. Therefore, the anatomy of the phantoms had great influence on the results. For example, considering the CC conversion of the thyroid, the values for the female phantom were affected by the presence of a thick layer of adipose tissue, which was not the case for the male phantom.

As for dose delivery in the target tissue, many authors recommend the use of high-energy beams for bone marrow ablation. However, it was not possible to observe that the calculated CCs for this organ reflected a more realistic behavior for the spectra above 10 MV by limiting the dose response functions used for dose estimation at the bone sites. Despite this, the method provided good results for the 4, 6 and 10 MV beams.

As expected, the presence of the attenuators leaded to reduction of CC of most of the organs in front of which the lead blocks are positioned. For superficial organs/tissues, such as the male breasts and the skin, the shielding leaded to increased CC.

The Conversion Coefficients of the effective dose per air kerma were higher for the AP irradiation geometry due to the fact that the more radiosensitive organs presented a high-energy absorption (breasts, for example). When the attenuators were inserted in the scenarios these coefficients showed a decrease for all irradiation geometries, even though the organs of the abdominal and pelvic region were not influenced, as evidenced by the Mesh Tally.

Acknowledgement

The authors acknowledge the Universidade Federal de Sergipe (UFS), the Coordenação de Aperfeiçoamento de Pessoal de Nível Superior (CAPES), the Conselho Nacional de Desenvolvimento Científico e Tecnológico (CNPq) and the Instituto Nacional de Metrologia das Radiações na Medicina (INCT) for the partial financial support of this study.

References

Van Dyk, J., Galvin, J.M., Glasgow, G.P., Podgorsak, E.B., 1986. AAPM 17 -The physical aspects of total and half body photon irradiation.

Bailey, D.W., Wang, I.Z., Lakeman, T., Hales, L.D., Singh, A.K., Podgorsak, M.B., 2015. TBI lung dose comparisons using bilateral and anteroposterior delivery techniques and tissue density corrections. J. Appl. Clin. Med. Phys. 16, 291–301. https://doi.org/10.1120/jacmp.v16i2.5293.

Chakarova, R., Müntzing, K., Krantz, M., Hedin, E., Hertzman, S., 2013. Monte Carlo optimization of total body irradiation in a phantom and patient geometry. Phys. Med. Biol. 58, 2461–2469. https://doi.org/10.1088/0031-9155/58/8/2461.

Corns, R., Evans, M., Olivares, M., Dyke, L., Podgorsak, E.B., Freeman, C.R., 2000. Designing attenuators for total-body irradiation using virtual simulation. Med. Dosim. 25, 27–31. https://doi.org/10.1016/S0958-3947(99)00038-2.

El-Khatib, E., Connors, S., Logus, W., 1992. The influence of lung and bone dosimetry on the choice of radiation energy for total body irradiation. Int. J. Radiat. Oncol. Biol. Phys. 23, 1051–1057. https://doi.org/10.1016/0360-3016(92)90913-3.

Ganapathy, K., Kurup, P.G.G., Murali, V., Muthukumaran, M., Bhuvaneshwari, N., Velmurugan, J., 2016. Patient dose analysis in total body irradiation through in vivo dosimetry. J. Med. Phys. 37, 214–218. https://doi.org/10.4103/0971-6203.103607.

ICRP 89, 2002. Basic anatomical and physiological data for use in radiological protection: reference values. In: Annals of the ICRP. ICRP. https://doi.org/10.1016/S0146-6453(03)00002-2.

ICPR, 2010. Conversion Coefficients for radiological protection quantities for external radiation exposures. In: Annals of the ICRP. Annals of the ICRP publication 116. https://doi.org/10.1016/j.icrp.2011.10.001.

ICRP, 2007. The 2007 recommendations of internacional commision on radiological protection. In: Annals of the ICRP. Annals of the ICRP publication 103. https://doi.org/10.1093/rpd/ncn187.

Jones, L.R., Toth, B.B., Keene, H.J., 1992. Effects of total body irradiation on salivary gland function and caries-associated oral microflora in bone marrow transplante patients. Oral Surg. Oral Med. Oral Pathol. 73, 670–676. https://doi.org/10.1016/0030-4220(92)90007-D.

Lamichhane, N., Patel, V.N., Studenskia, M.T., 2016. Going the distance: validation of acuros and AAA at an extended SSD of 400 cm. J. Appl. Clin. Med. Phys. 17, 63–73. https://doi.org/10.1120/jacmp.v17i2.5913.

Lavallee, M.C., Aubin, S., Larochelle, M., Vallieres, I., Beaulieu, L., 2011. 3D heterogeneous dose distributions for total body irradiation patients. J. Appl. Clin. Med. Phys. 12, 3416.

Lee, C., Lee, C., Lodwick, D., Bolch, W.E., 2007. NURBS-based 3-D anthropomorphic computational phantoms for radiation dosimetry applications. Radiat. Prot. Dosim. 127, 227–232. https://doi.org/10.1093/rpd/ncm277.

Lee, C., Lodwick, D., Hurtado, J., Pafundi, D., Williams, J.L., Bolch, W.E., 2010. The UF family of reference hybrid phantoms for computational radiation dosimetry. Phys. Med. Biol. 55, 339–363. https://doi.org/10.1088/0031-9155/55/2/002.

Linares, F.M., Papanikolaou, N., Esquivel, C., Eng, T.Y., Fuller, C.D., 2017. Prescribed and measured dose differences for an AP-PA TBI protocol with compensation filter and ergonomic patient support. J. Med. Imaging Radiat. Sci. 48, 301–306. https://doi.org/10.1016/j.jmir.2017.06.001.

Mesa, F., Eng, T.Y., Esquivel, C., Fuller, C.D., Papanikolaou, N., Sosa, M., 2010. Implementation of a lateral total body irradiation technique with 6 MV photons: the University of Texas health science center in San Antonio experience. J. Radiother. Pract. 1–10. https://doi.org/10.1017/S1460396910000221.

Narayanasamy, G., Cruz, W., Saenz, D.L., Stathakis, S., Papanikolaou, N., Kirby, N., 2016. Effect of electron contamination on in vivo dosimetry for lung block shielding during TBI. J. Appl. Clin. Med. Phys. 17, 486–491. https://doi.org/10.1120/jacmp.v17i3.6128.

Ounoughi, N., Mavon, C., Belafrites, A., Fromm, M., 2015. Spatial distribution of air kerma rate and impact of accelerating voltage on the quality of an ultra soft X-ray beam generated by a cold cathode tube in air. Radiat. Meas. 80, 23–28. https://doi.org/10.1016/j.radmeas.2015.07.001.

Pelowitz, D.B., 2011. MCNPX User's Manual Version 2.7. Los Alamos National Laboratory.

Quast, U., Total body irradiation- review of treatment techniques in Europe. 9. 1987. 91–106.

Sheikh-Bagheri, D., Rogers, D.W.O., 2002. Monte Carlo calculation of nine megavoltage photon beam spectra using the BEAM code. Med. Phys. 29, 391–402. https://doi.org/

10.1118/1.1445413.
Soto-Bernal, T.G., Baltazar-Raigosa, A., Medina-Castro, D., Veja-Carrillo, H.R., 2017. Neutron production during the interaction of monoenergetic electrons with a Tungsten foil in the radiotherapeutic energy range. Nucl. Instrum. Methods Phys. Res. A 868, 27–38. https://doi.org/10.1016/j.nima.2017.06.027.
Thomas, O., Mahé, M., Campion, L., Bourdin, S., Milpied, N., Brunet, G., Lisbona, A., Le Mevel, A., Moreau, P., Harousseau, J., Cuillière, J., 2001. Long-term complications of total body irradiation in adults. Int. J. Radiat. Oncol. Biol. Phys. 49, 125–131. https://doi.org/10.1016/S0360-3016(00)01373-0.
X-5 Monte Carlo Team, 2003. MCNP — A general Monte Carlo N-Particle transport code, version 5. In: Overview and Theory. 1 Los Alamos National Laboratory.
Xu, X.G., Eckerman, K.F., 2010. Handbook of Anatomical Models for Radiation Dosimetry. Taylor and Francis Group, USA.
Yao, R., Bernard, D., Turian, J., Abrams, R.A., Sensakovic, W., Fung, H.C., James, C.H., 2012. A simplified technique for delivering total body irradiation (TBI) with improved dose homogeneity. Med. Phys. 39, 2239–2248. https://doi.org/10.1118/1.3697526.